

EFFECTS OF HALO TRIAXIALITY, ANISOTROPY AND SMALL SCALE CLUMPING ON WIMP DIRECT DETECTION EXCLUSION LIMITS

ANNE M GREEN

*Physics Department, Stockholm University,
Stockholm, 10691, SWEDEN
E-mail: amg@physto.se*

Weakly Interacting Massive Particle (WIMP) direct detection experiments are closing in on the region of parameter space where neutralinos may constitute the Galactic halo dark matter. Numerical simulations and observations of galaxy halos indicate that the standard Maxwellian halo model is likely to be a poor approximation to the dark matter distribution. We examine how halo models with triaxiality and/or velocity anisotropy affect exclusion limits, before discussing the consequences of the possible survival of small scale clumps.

1. Milky Way halo modelling

Current Weakly Interacting Massive Particle (WIMP) direct detection experiments are just reaching the sensitivity required to detect Galactic dark matter in the form of neutralinos. The direct detection event rate and its energy distribution are determined in part by the WIMP speed distribution, with data analyses nearly always assuming a standard spherical halo model with isotropic Maxwellian velocity distribution.

Observational constraints on the form of dark matter halos depend on the relation of luminous tracer populations to the underlying density distribution, and are complicated by galactic structure and projection effects, however it appears that galaxy halos are triaxial (for a review see Ref. ¹). In particular for the Milky Way, analysis of local stellar kinematics gives an estimate for the short-to-long axis ratio of 0.7 ± 0.1 ², while the great circle tidal streams observed from the Sagittarius dwarf galaxy rule out a ratio of less than 0.7 in the outer halo ³ (in a flattened potential angular momentum is not conserved, so that orbits precess and tidal streams lose their coherence). Given the difficulties involved in ‘observing’ dark matter halos it makes sense to turn to numerical simulations for information on

their possible properties. In CDM cosmologies structure forms hierarchically; small objects (often known as subhalos) form first, with larger objects being formed progressively via mergers and accretion. The shape and internal structure of galaxy size halos are then determined by the dynamical processes which act on the component subhalos.

The shape of simulated halos varies, not just between different halos of the same mass, but also as a function of radius within a single halo, strongly if the halo has undergone a major merger relatively recently. Two high resolution Local Group halos studied in detail in Ref. ⁴ have axis ratios of $1 : 0.78 : 0.48$ and $1 : 0.45 : 0.38$ at the solar radius. Adding dissipative gas to simulations tends to preserve the short-to-long axis ratio while increasing the intermediate-to-long axis ratio ⁵.

The anisotropy parameter $\beta(r)$, defined as

$$\beta(r) = 1 - \frac{\langle v_\theta^2 \rangle + \langle v_\phi^2 \rangle}{2 \langle v_r^2 \rangle}, \quad (1)$$

where $\langle v_\theta^2 \rangle$, $\langle v_\phi^2 \rangle$ and $\langle v_r^2 \rangle$ are the means of the squares of the velocity components, also varies with radius. Typically $\beta(r)$ grows, although not monotonically, from roughly zero in the centre of the halo to close to one at the virial radius, with non-negligible variation between halos. The high resolution galactic mass halos studied in Ref. ⁶ have $\beta(R_\odot)$ in the range 0.1-0.4, which corresponds to radially biased orbits.

2. Effect on exclusion limits

The differential WIMP event rate due to scalar interactions can be written in terms of the WIMP scattering cross section on the proton, σ_p :

$$\frac{dR}{dE} = \zeta \sigma_p \left[\frac{\rho_{0.3}}{2} \frac{(m_p + m_\chi)^2}{m_p^2 m_\chi^3} A^2 F^2(q) \int_{v_{\min}}^{\infty} \frac{f_v}{v} dv \right], \quad (2)$$

where the local WIMP density, ρ_χ , is normalised to a fiducial value $\rho_{0.3} = 0.3 \text{ GeV/cm}^3$ such that $\zeta = \rho_\chi / \rho_{0.3}$, A and $F(q)$ are the atomic number and form factor of the target nuclei, f_v is the WIMP speed distribution in the rest frame of the detector, normalised to unity, and v_{\min} is the minimum WIMP speed which can produce a recoil of energy E : $v_{\min} = (E(m_\chi + m_A)^2 / 2m_\chi^2 m_A)^{1/2}$.

We will consider the two self-consistent triaxial and/or anisotropic halo models which have been studied in relation to WIMP direct detection to date: the logarithmic ellipsoidal model ⁷ and the Osipkov-Merritt anisotropy model ⁸, studied in Ref. ⁹. The logarithmic ellipsoidal model ⁷

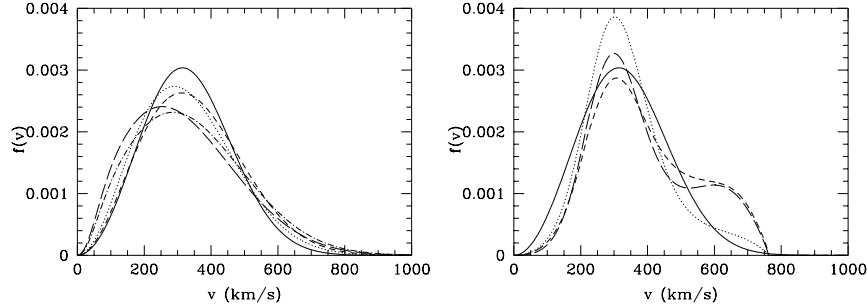


Figure 1. The speed distributions, in the rest frame of the Sun, for the standard halo model (solid line), and the logarithmic ellipsoidal model on the intermediate axis (left panel) for parameters which produce axis ratios 1 : 0.78 : 0.48 and $\beta = 0.1/0.4$ (dotted/short dashed) and for axis ratios 1 : 0.45 : 0.38 and $\beta = 0.1/0.4$ (long dashed/dot dashed) and for the OM model (right panel) with anisotropy radii which produce $\beta(R_\odot) = 0.13, 0.31$ and 0.4 (dotted, short-dashed, and long-dashed).

is the simplest triaxial generalisation of the isothermal sphere and on either the long or the intermediate axis the velocity distribution can be approximated by a multi-variate gaussian. Speed distributions on the intermediate axis, in the rest frame of the Sun normalised to unity, are plotted in Fig. 1 along with that for the standard Maxwellian halo model. The logarithmic ellipsoidal model has a wider spread in speeds than the standard model, so that the differential event rate decreases less rapidly with increasing recoil energy.

In the Osipkov-Merritt (OM) model ⁸, which assumes a spherically symmetric density profile, the velocity anisotropy varies as a function of radius as $\beta(r) = r^2/(r^2 + r_a^2)$ so that the degree of anisotropy increases with increasing radius, as is found in numerical simulations. Following Ref. ⁹ we assume a NFW density profile with scale radius $r_s = 20$ kpc. We use values of the anisotropy radius r_a which correspond to $\beta(R_\odot) = 0.14, 0.31$ and 0.4 . The resulting speed distributions are plotted in Fig. 1.

In Fig. 2 we plot the exclusion limits found from the IGEX data ¹⁰, taking into account the detector resolution, for the logarithmic ellipsoidal model and for the OM model. We also plot the exclusion limits from the Heidelberg-Moscow (HM) experiment ¹¹ for the OM model in Fig. 3. Comparing Figs. 2 and 3 we see that the change in the exclusion limits depends not only on the halo model under consideration, but also on the data being used; for IGEX the change in the exclusion limits is largest for

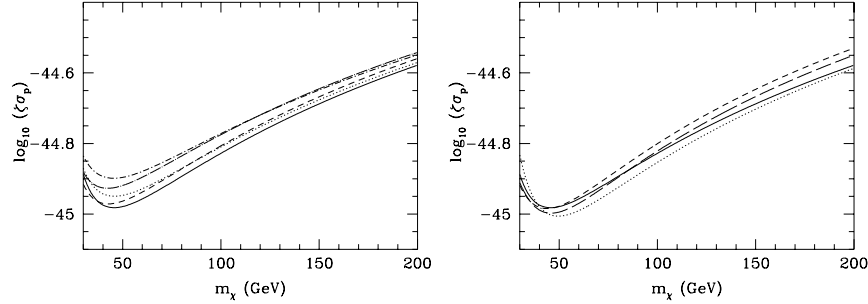


Figure 2. The exclusion limits from the IGEX experiment for the logarithmic ellipsoidal model, location on the intermediate axis (left panel) and for the OM model (right panel).

large m_χ , while for HM the change is largest for small m_χ . This is because for different m_χ , different energy ranges can be most constraining; for the IGEX data the lowest energy bin is always the most constraining, while for HM as m_χ increases the constraint comes from higher energy bins. It should therefore be borne in mind when comparing exclusion limits from different experiments, that changing the assumed WIMP speed distribution will affect the limits from different experiments differently.

The changes in the exclusion limits are not huge (of order tens of percent) for the experiments we have considered, however these experiments are not optimised for WIMP detection. The change in the differential event rate, and hence the exclusion limit, would be larger for an experiment with better energy resolution and lower threshold energy (see Ref. ¹²). We have also seen that different models with the same value for the anisotropy parameter β can have very different speed distributions, and hence a different effect on the exclusion limits. Furthermore it is conceivable that the local WIMP speed distribution may deviate even further from the standard Maxwellian distribution than the models that we have considered.

3. Small scale clumping

Numerical simulations are an extremely powerful tool for understanding the large scale structure of the universe, however the local dark matter distribution, which is crucial for direct detection experiments, can not be probed directly by cosmological simulations. The smallest subhalos resolvable in the highest resolution simulations have mass of order $10^7 M_\odot$, while the first bound neutralino clumps to form would have mass, at matter-

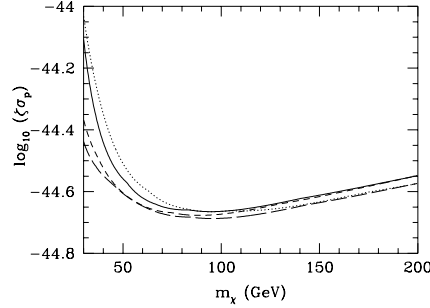


Figure 3. The exclusion limits from the HM experiment for the OM model.

radiation equality, $\sim 10^{-7} M_{\odot}$ ¹³. Other approaches^{14,4,15} have therefore been used to address the problem, with the results obtained depending on the method used to extrapolate to small scales below the resolution limit of the cosmological simulations^a. Moore et al. claim that the phase space distribution at the solar radius will depend crucially on the Galaxy’s merger history and on the internal structure of the smallest subhalos, arguing that it is possible that the local dark matter density could be zero, or that a single dark matter stream with small velocity dispersion could dominate, or that many tidal streams could overlap to give a smooth distribution.

We will now discuss the consequences for the WIMP direct detection rate if small dense clumps survive at the solar radius. We emphasise that it is not clear at the moment whether this is the case, and further work is necessary to clarify this issue. We could then be currently located within a clump with local density in excess of the mean value, on the other hand it is possible that we could be in a region between clumps where the WIMP density is zero⁴. In the latter case all current attempts at WIMP direct detection would be doomed to failure^b, and exclusion limits would tell us nothing about the WIMP cross-section. At the other extreme a dense clump at the earth’s location would produce an enhanced event rate and a distinctive experimental signal (the theoretical differential event rate would be a step function with amplitude inversely proportional to the speed of the subhalo with respect to the earth, and position increasing with increasing relative speed and WIMP mass). For small clump velocities and

^aSee Ref. ¹² for a more extensive discussion.

^bWIMPs could still be detected using ancient mica though as it has an integration time of order a Gyr¹⁶.

WIMP masses there would be no constraint on the WIMP cross-section (no WIMPs would have sufficient energy to cause an observable recoil), but as the WIMP mass is increased the constraints would become much tighter as then all the WIMPs would be energetic enough to cause events of a given recoil energy.

4. Conclusions

We have seen that even if the local WIMP distribution is smooth its velocity distribution may deviate significantly from the standard Maxwellian, and this has a non-negligible effect on exclusion limits from WIMP direct detection experiments, affecting the limits from different experiments differently. The effect on experiments which can detect the angular and/or time variation of the event rate will be more significant. Constraints (and in the future possibly best fits) calculated assuming a standard Maxwellian halo could be erroneous, even worse if only the signals expected from the standard halo model (e.g. a sinusoidal annual modulation with peak in June) are searched for, a real WIMP signal could be overlooked. On the other hand, more optimistically, if WIMPs were detected it might then be possible to derive useful information about the local velocity distribution, and hence the formation of the Galactic halo.

References

1. P. D. Sackett, astro-ph/9903420.
2. R. P. Olling and M. R. Merrifield, MNRAS **311**, 361 (2000).
3. R. Ibata, G. F. Lewis, M. Irwin, E. Totten and T. Quinn, ApJ **551**, 294 (2001).
4. B. Moore et al., Phys. Rev. D **64**, 063508 (2001).
5. N. Katz and J. E. Gunn, ApJ **377**, 365 (1991); J. Dubinski, ApJ **431**, 617 (1994).
6. B. Moore et al., MNRAS **310**, 1147 (1999).
7. N. W. Evans, C. M. Carollo and P. T. de Zeeuw, MNRAS **318**, 1131 (2000).
8. L. P. Osipkov, Pis'ma Astron. **55**, 77 (1979); D. Merritt, AJ **90**, 1027, (1985).
9. P. Ullio and M. Kamionkowski, JHEP 0103:049 (2001).
10. A. Morales et al., Phys. Lett. B **532**, 8 (2002).
11. L. Baudis et al., Phys. Rev D **59**, 022001 (1999).
12. A. M. Green, astro-ph/0207366 to appear in Phys. Rev. D.
13. S. Hofmann, D. J. Schwarz and H. Stoecker, Phys. Rev. D **64**, 083507 (2001).
14. D. Stiff, L. M. Widrow and J. Frieman, Phys. Rev. D **64**, 083516 (2001).
15. A. Helmi, S. D. M. White and V. Springel, Phys. Rev. D **66**, 063502 (2002).
16. D. P. Snowden-Ifft, E. S. Freeman and P. B. Price, Phys. Rev. Lett. **74**, 4133 (1995); E. A. Baltz, A. J. Westphal and D. P. Snowden-Ifft, Phys. Rev. D **59**, 023510 (1999).